

Wireless propagation in urban environments: modeling and experimental verification

Danilo Erricolo, Piergiorgio L.E. Uslenghi(*), Ying Xu, Qiwu Tan
Department of Electrical and Computer Engineering
University of Illinois at Chicago
851 S. Morgan St, Chicago, IL, 60607-7053, USA
email: derricol@ece.uic.edu, uslenghi@uic.edu

1 Introduction

Wireless communication systems play an important role in our society not only for voice transmission but also for data communications. New applications are constantly being developed and they usually result in a demand for higher transfer data rates. Therefore the design of reliable communication systems must be made with advanced engineering tools that account for the complex environment where communications take place so that higher data rates can be guaranteed. To achieve these data rates, one of the tasks that need to be accomplished is the proper characterization of the communication channel.

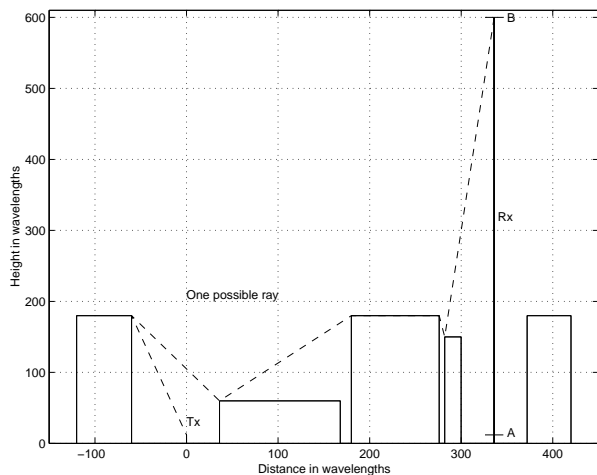
In order to obtain a characterization of the communication channel, one must be able to describe the propagation of electromagnetic waves in the environment under consideration. At the beginning of radio communications, one of the main concerns was propagation past large obstacles, such as hills or mountain ridges, and around the earth. Diffraction is the mechanism that explains the propagation around obstacles. In order to take advantage of the classical solution for the problem of diffraction past a half plane, many earlier works have assimilated large obstacles to knife edges. Later, propagation problems have been successfully studied with a simplification of the wave equation that leads to the parabolic-equation method. These different methods are described in, among other works, [1], [2], [3], [4], [5], [6], [7].

In this presentation, using ray-tracing methods, we examine the efforts that have been taken by our research group in order to provide effective models to characterize the propagation of electromagnetic fields inside urban environments. We first describe our polygonal line simulator for the analysis of electromagnetic wave propagation in a vertical plane. We then discuss its accuracy by showing the results of measurements that were taken in the frequency-domain and in the time-domain. Next the polygonal line simulator is compared with the methods of Hata, Zhang and COST-231. Then a general method to address propagation in a horizontal 2D environment is explained. Finally, we present a new 3D propagation method that is currently under development within our research group.

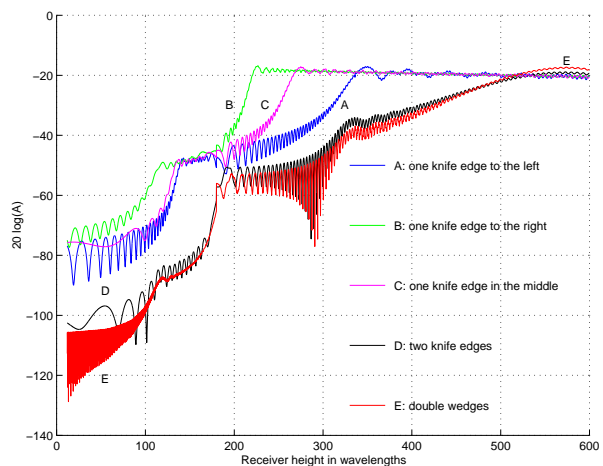
2 The polygonal line simulator

This two-dimensional simulator analyzes the path loss experienced by electromagnetic waves that propagate through the obstacles of an urban environment using ray-tracing methods. Because it is a two-dimensional simulator, only the trajectories that are contained in a vertical plane passing through the transmitter and the receiver are considered. In addition, it is assumed that the vertical plane is normally incident on the walls of the buildings between the antennas. The profile of the obstacles that are cut by the vertical plane is represented by a polygonal line, so that both variations of the height of the terrain and complex building shapes are taken into account. The new algorithm introduced into this simulator calculates all the rays that propagate along a vertical plane from the transmitter to the receiver, neglecting any backscattered ray.

Reflections can occur either on the terrain or along building surfaces. Diffractions are calculated using the Uniform Theory of Diffraction (UTD) [8] and its extensions designed to account for scattering by impedance wedges. Each segment of the polygonal profile is associated with its own value of surface impedance so that varying electrical characteristics for both terrain and building surfaces are accounted for. One advantage of using a polygonal



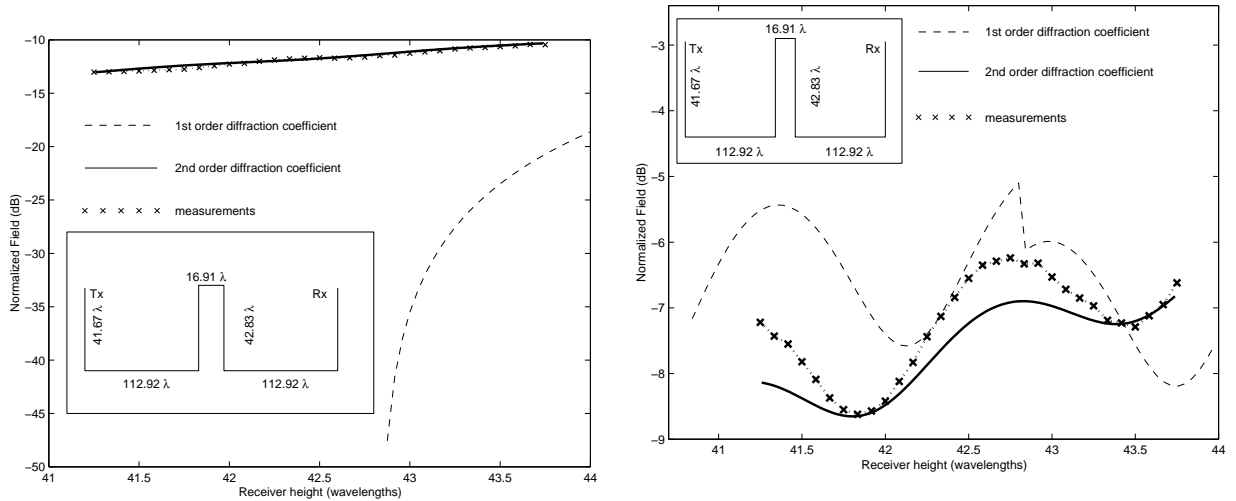
(a) Profile for buildings approximated using double wedges



(b) Overall attenuation for the profile of Fig. 1(a) using different building models in the case of hard boundary. Results are shown for: A) One knife edge to the left; B) One knife edge to the right; C) One knife edge in the middle; D) Two knife edges; E) Double wedges.

Figure 1: Rectangular shapes vs knife edges to approximate buildings

line is that buildings may be modelled using a rectangular shape [9]. The advantage of using a rectangular shape over a knife edge becomes clear as shown in Fig. 1. In fact, when one of the buildings of Fig. 1(a) is replaced with a knife edge, some possible choices are A) locate a knife edge at the left wall of each building; B) locate a knife edge at the right wall of each building; C) locate a knife edge at the center of each building; and D) locate two knife edges one at the left wall and the other at the right wall of each building. All knife edges have the same height of the building that they approximate. It is worth noting that choices A) and



(a) soft polarization. Mean error: 0.14 dB, standard deviation 0.08 dB

(b) hard polarization. Mean error: 0.36 dB, standard deviation 0.27 dB

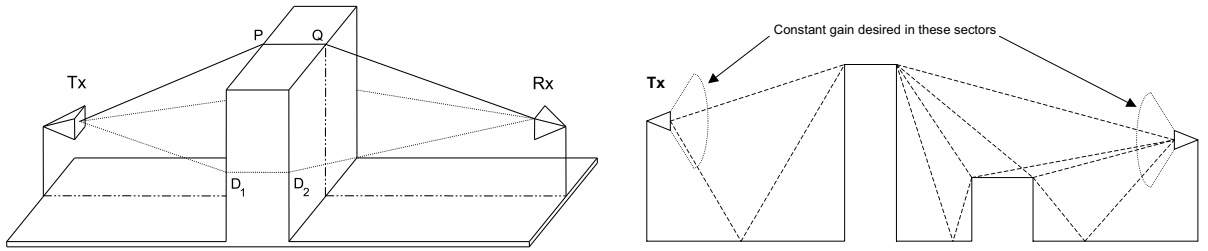
Figure 2: Advantages of the use of double diffraction coefficients

B) violate the reciprocity principle, since if T_x is switched with R_x the new situation is not reciprocal of the previous one. An automatic ray tracing for the profile shown in Fig. 1(a) was carried out and the receiver height was varied from A to B at small increments of $\lambda/10$ each. The results for perfect electrical conductor buildings and hard boundary are shown in Fig. 1(b).

The choice of rectangular shapes to approximate buildings must go together with the use of appropriate diffraction coefficients [10]. Specifically, one of the advantages of this simulator is the implementation of the diffraction coefficients for double wedges developed by Albani et al. [11] and those for impedance wedges of Herman and Volakis [12]. The importance of correctly characterizing double wedges is seen referring to Fig. 2, which shows the comparison among measurements and predictions computed using cascaded single order diffraction coefficients and double wedge diffraction coefficients. These results point out that the use of cascaded diffraction coefficients for soft polarization, Fig. 2(a), and hard polarization, Fig. 2(b), leads to errors, particularly for soft polarization.

2.1 Anechoic chamber experiments to measure the accuracy of the prediction

The novelty of these studies is that the measurements are conducted inside the anechoic chamber facility at the University of Illinois at Chicago, using scaled models of urban environments and appropriate antennas. The advantage of this approach is that all parameters such as physical dimensions of the model and material properties are known with very low tolerances. Therefore, it is possible to make extremely accurate comparisons with the theoretical prediction obtained using a ray-tracing method. The experiments must approximate, as closely as possible, the two-dimensional assumption. In particular, the trajectories considered by the polygonal line simulator are contained in a vertical plane. As a consequence,



(a) Example of three-dimensional propagation. The trajectory $T_x \rightarrow P \rightarrow Q \rightarrow R_x$ that is contained in the vertical plane is of interest for the experiments; however, the trajectory $T_x \rightarrow D_1 \rightarrow D_2 \rightarrow R_x$ is an undesired one.

(b) Example of the angular sectors within which the directive gain must be as constant as possible to guarantee that all trajectories of interest are equally weighted.

Figure 3: 3D trajectories and vertical pattern requirements

in order to experimentally emphasize only those trajectories that are contained in the vertical plane, such as trajectory $T_X \rightarrow P \rightarrow Q \rightarrow R_X$ of Fig. 3(a), the patterns of both antennas in the horizontal plane must be narrow and directed along the line connecting the antennas. Furthermore, for both antennas the directivity patterns in the vertical plane must be isotropic, so that the contributions from all possible trajectories are equally weighted. At least within the angular sector of interest shown in Fig. 3(b), the directivity gain must be reasonably constant. The experiments measure the field $E(R_x)$ that reaches R_x after propagating past the scaled building models. During the experiments, T_x is fixed while R_x is manually moved vertically. Measurement data are plotted in terms of the normalized field $E_0(R_x)$, i.e the measured field $E(R_x)$ divided by the magnitude of the field measured for the same position of the antennas in free space $E_{\text{free space}}(R_x)$:

$$E_0(R_x) = \frac{E(R_x)}{|E_{\text{free space}}(R_x)|}. \quad (1)$$

Two polarizations are considered: hard (Neumann boundary condition) and soft (Dirichlet boundary condition). The geometrical shapes of the scaled models are simple but effective to test the performance of the polygonal line simulator. Further details of this investigation were given in [13].

2.1.1 Frequency domain measurement

As an example of these measurements we consider the two-building profile that may be regarded as the simplest case of multiple rows of buildings having nearly uniform height, which is a situation of practical interest, especially in suburban areas. The case of two buildings of almost equivalent height is challenging for any ray-tracing method.

Referring to the inset of Fig. 4, the challenge comes from the trajectories that illuminate the building to the left and are diffracted towards the building to the right. These trajectories are in the transition zone of the edges and, therefore, the application of the ray-tracing method must be verified. In particular, the most difficult case occurs when the transmitter is below the building rooftop since the field at the receiver is only due to diffraction mechanisms, which have to be carefully computed. This explains why the configurations that were

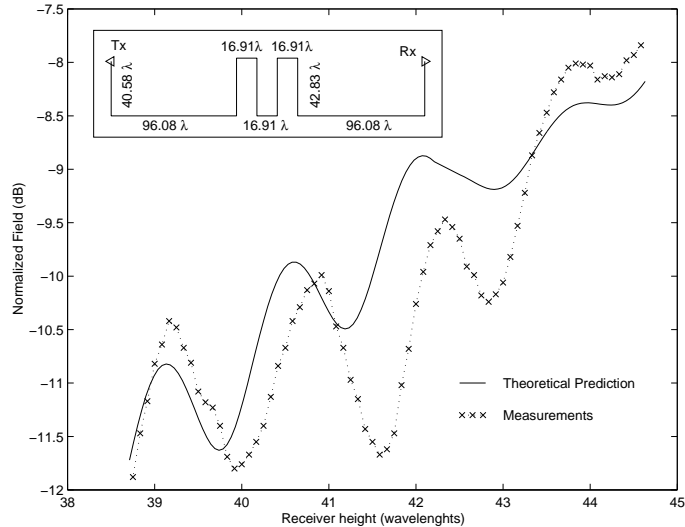


Figure 4: Propagation with Tx below rooftops. Hard polarization case for grazing observation aspect with an incidence angle is 1.34° . For these data, the mean error is 0.59 dB and the standard deviation is 0.50 dB.

measured consider the transmitter either below the rooftop or slightly below the rooftop to cause grazing incidence.

In particular, here we examine the configuration depicted in the inset of Fig. 4 that causes the transmitter to create grazing incidence. In fact, in Fig. 4, the trajectory that impinges the left edge of the left building makes an angle of 2.18° with the line through the building rooftops, whereas in Fig. 4 the same angle is reduced to 1.13° . Fig. 4 shows the details of this comparison and corresponds to a mean error of 0.59 dB and a standard deviation of 0.50 dB. Improvements could be achieved using higher order diffraction coefficients, but the benefits would be far too small when compared to the increased computational effort.

2.1.2 Time domain measurement

The purpose of the TD analysis is the measurement and identification of the multipath components that actually contribute towards the received field in a selected frequency band. This requires the ability to resolve two closely time spaced multipath components, which we will refer to as *response resolution*, and the ability to locate the peak, in time, of a single multipath component, which we will refer to as *range resolution*. The experiments consist of pulses that are launched from T_x and measured at R_x .

For a given scaled model of an urban environment, different configurations are considered. Each configuration is characterized by the positions of the transmitter and receiver with respect to the scaled building model. Given a certain configuration as input, the PL simulator computes the complex value of the EM field for a pre-determined set of frequencies. Both the experiments and the theoretical predictions return results in the frequency domain. The TD analysis was accomplished via post-processing using MATLAB.

Similarly to what we already examined in the frequency-domain case, the TD analysis of the multipath components is now applied to the case of the two-building profile. This profile

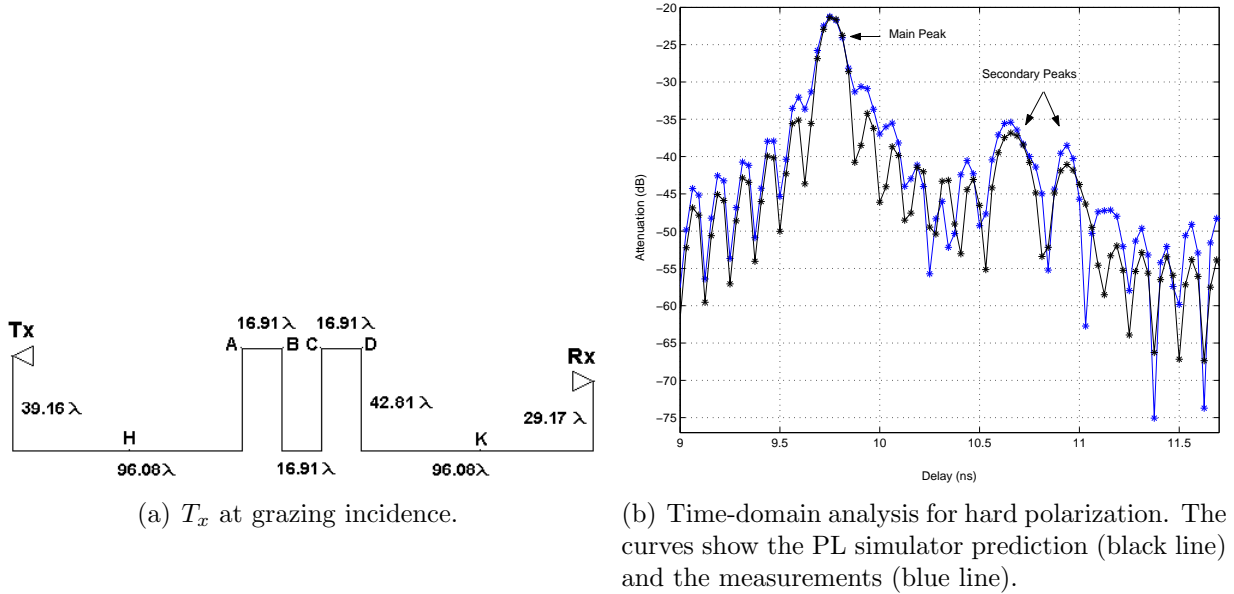


Figure 5: Time-domain analysis

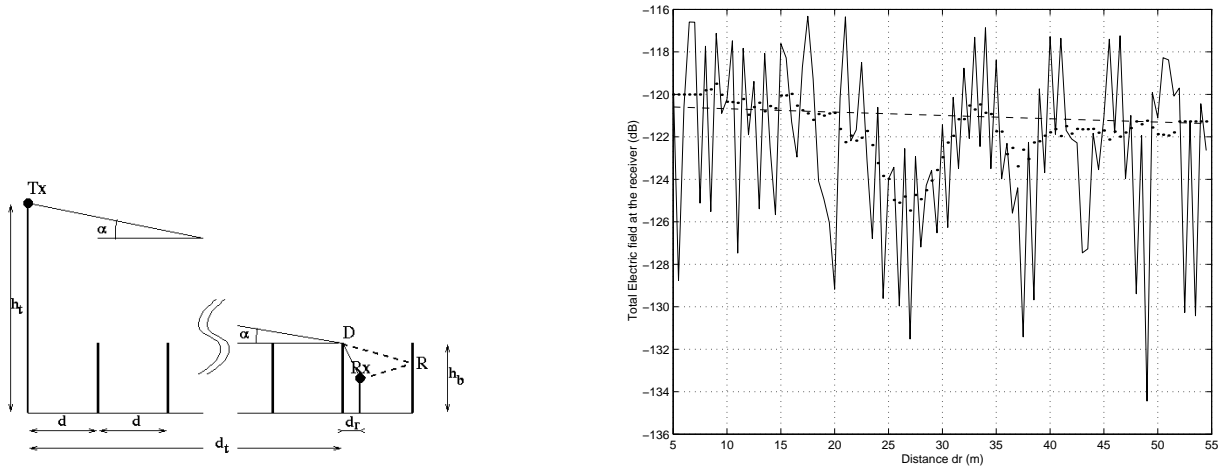
represents the simplest case of rows of parallel buildings. In addition, since the two buildings have exactly the same height, it provides a way to challenge the ray-tracing algorithm because of the intrinsic grazing incidence condition created by this particular shape. Further details are given in [14]. As an example, Figure 5(a) shows the geometry for the configuration of the T_x at grazing incidence. For this configuration, the trajectories that provide the most important contributions are:

1. $T_x \rightarrow A \rightarrow B \rightarrow C \rightarrow D \rightarrow R_x$
2. $T_x \rightarrow A \rightarrow B \rightarrow C \rightarrow D \rightarrow K \rightarrow R_x$
3. $T_x \rightarrow H \rightarrow A \rightarrow B \rightarrow C \rightarrow D \rightarrow R_x$

The TD analysis is shown in Figure 5(b), which corresponds to a hard-polarization case. Hard polarization was chosen because it results in stronger values for the received field and therefore makes the measurements easier.

Table 1: Configuration 3: Comparison between measured data and predictions given by the PL simulator.

Trj	Measured Delay (ns)	Data Attn (dB)	PL Delay (ns)	Simul Attn (dB)
1	9.750	-21.25	9.763	-21.36
2	10.655	-35.40	10.680	-36.84
3	10.934	-38.65	10.964	-41.07



(a) Geometry for a simplified urban environment where buildings are replaced using knife edges. The continuous line represents a diffracted path, whereas the dashed line represents a diffracted-reflected path.

(b) Comparison with COST-231 Walfisch-Ikegami model. The solid line represents the polygonal line simulator; the dashed line is the COST-231 Walfisch-Ikegami model; and the dotted line represents the local average of the polygonal simulator results. Simulation data for this comparison are given in Table 2. d_r varies at increments of 0.5 m, which corresponds to 3.6 wavelengths.

Figure 6: Comparison with COST-231 for knife-edge buildings

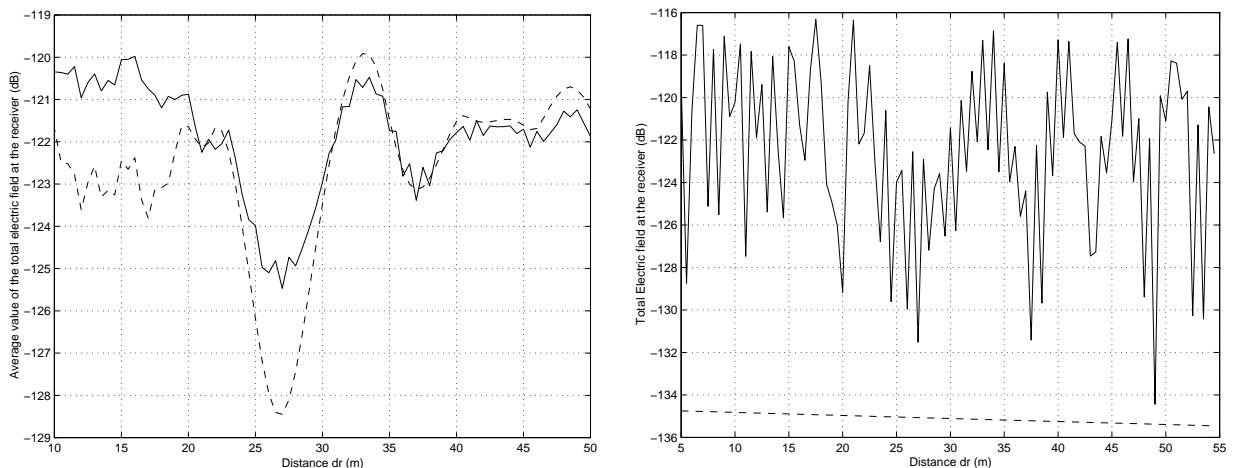
The main peak of Figure 5(b) is easily identified with trajectory 1 of Table 1. The agreement with the theoretical prediction is very good both for the main and the secondary peaks. Also, trajectories 2 and 3 provide similar contributions.

2.2 Comparison with Cost-231, Zhang and Hata

Many models for propagation in urban environment represent building obstructions using the knife edge approximation, as reported, for example, in [15] [16] [17] [18] [19]. Therefore the geometry of Fig. 6(a) is considered herein to compare different propagation prediction methods because it represents an urban environment where parallel rows of buildings are modelled using knife edges. In the configuration of Fig. 6(a), the transmitter Tx is always above the rooftop height and the receiver is always in an obstructed area. Further details are provided in [20]. A comparison of the prediction obtained with the polygonal line simulator and the COST-231 Walfisch-Ikegami model is shown in Fig. 6(b). For this comparison, as well as for those shown in Fig. 7(a) and 7(b), the geometry of the environment under study is shown in Fig. 6(a) and the parameters for the simulation are shown in Table 2. The comparison is carried out by computing the total electric field at the receiver, while the receiver moves horizontally and d_r measures its distance from the knife edge to its left. The total field is calculated assuming an isotropic source with transmitted power $P_t = 1\text{W}$ and vertical polarization. Referring to Fig. 6(b), the prediction obtained using the COST-231 Walfisch-Ikegami model is in agreement with the one of the polygonal line simulator. In fact, the average value of the difference between the two curves is 1.46 dB and the standard

Table 2: Parameters for the geometry of Fig. 6(a)

Parameter	Value
frequency	f=2.154 GHz
transmitter height	$h_t = 12$ m
building separation	d=60 m
horizontal distance between T_x and D	$d_t=1020$ m
distance from mobile to left building	$5 \leq d_r \leq 55$ m
mobile height	$h_r=1.6$ m
building height	$h_b=10$ m
relative dielectric permittivity	$\varepsilon=5$
knife edges between T_x and R_x	n=17



(a) Comparison between the average values of the two-dimensional simulator (continuous line) and Zhang's method (dashed line).

(b) Comparison with Hata's model. The solid line is the polygonal line simulator result; the dashed line is Hata's model result.

Figure 7: Comparison with Hata's method for knife-edge buildings

deviation of this difference is 4.0 dB. In this comparison, the correction to the COST-231 Walfisch-Ikegami model described in [21] was introduced. The next comparison is with the method of Zhang and the corresponding result is shown in Fig. 7(a). The parameters for this comparison are reported in Table 2 and for the simplified geometry under examination, there is good agreement between the two predictions: the difference between the average values of the two predictions never exceeds 3 dB.

Finally a comparison is given with Hata's model [22] in Fig. 7(b). The average difference between the two curves is 12.6 dB and the standard deviation of the difference is 4.0 dB, a result that shows Hata's prediction is too pessimistic. The difference between Hata's prediction and the polygonal line simulator may be explained on the basis that Hata's model was obtained by fitting the experimental data measured by Okumura [23] and using only a few parameters to describe the environment.

3 A general method to study 2D propagation

Electromagnetic wave propagation in urban environments among high-rise buildings may be described using trajectories that propagate around buildings instead of over them. This problem may be simplified by modelling the environment with polygonal cross-section buildings that are infinitely high and by assuming that propagation takes place in a plane perpendicular to the buildings. With these simplifications, the problem is reduced to the scattering of a cylindrical wave incident on a group of two-dimensional polygonal cylinders. The goal of this study is the evaluation of the field intensity at an arbitrary observation point, while accounting for the interaction of the cylindrical wave with the polygonal obstacles. The study is carried out using ray tracing methods, which implies the determination of all the trajectories connecting the source point to the observation point. The approach taken consists of:

- Preprocessing the information related to the position of the polygonal cylinders. This operation is carried out to establish the "local" visibility that each polygon has in relation to its neighbors.
- The construction of an overall visibility graph using the results found in the previous step.
- The extraction of the ray trajectories connecting the source point to the observation point by means of a traversal algorithm that is applied to the overall visibility graph.

For each ray trajectory, it must be verified that both geometrical optics (i.e., reflection law) and geometrical theory of diffraction (i.e., edge diffraction law) are fulfilled. Then the field strength at the observation point is computed by coherent superposition of the field strength associated with each ray trajectory. The field intensity of each ray trajectory is calculated by introducing the proper reflection and diffraction coefficients along the path. The electromagnetic properties of the polygonal cylinders are given in terms of surface impedance, which makes this study quite flexible in terms of the variety of situations that can be represented. Finally, the algorithm is implemented in C++ language to take full advantage of the methodologies offered by object-oriented programming. Further details are found in [24].

3.1 The Method

Free space propagation and reflection are easily treated with ordinary ray tracing methods. Diffraction cannot be studied using an ordinary ray tracing approach because of the law of edge diffraction according to which a ray incident on an edge creates a whole cone of diffracted rays. Therefore, an inverse method is used to avoid the problem of dealing with a cone of an infinite number of diffracted rays. The idea is to consider two points, the source and the observation, and to connect them with all the trajectories that it is possible to draw according with the constraints imposed by the environment. The polygons can be concave or convex and both their faces and vertices will be referred to as the scattering elements of the environment. Rays that propagate from the source to the observation point interact with the environment at the scattering elements. The interactions at the scattering elements are either reflections or diffractions. For a given ray trajectory, the number of interactions at

the scattering elements determines the order of the ray. Therefore, a direct ray from source to observation is a zero order path, whereas a ray that undergoes either one reflection or one diffraction during its propagation will be referred to as a first order path. The algorithm that will be presented can compute the trajectories under the assumption that a given path must not pass twice through the same point. The algorithm determines the trajectories starting from order zero up to a specified order. The first order trajectory is computed using the following steps:

1. All scattering elements that are visible from the source (i.e. all elements that have a line of sight with the source) are determined and collected together in what will be referred to as the visibility list of the source.
2. Each element of the visibility list that has a line of sight with the observation point is selected to become part of a candidate trajectory.
3. The candidate trajectory is composed of the source, the scattering element, and the observation point. If the scattering element is a vertex, where a diffraction occurs, then the trajectory passing through the scattering element is a physical trajectory. However, if the scattering element is a segment, one has to establish whether the angles of incidence and reflection satisfy the reflection law.

3.2 Determination of the visibility

One of the most difficult tasks to solve in this problem is the determination of the visibility in an environment with a potentially large number of objects. A statistics of ray tracing applications shows that, in order to render images where thousands of objects are present, more than 95% of the time is spent performing intersection calculations between rays and objects [25], if an exhaustive approach is taken. An exhaustive implementation is prohibitive and before implementing any ray tracing algorithm it is necessary to become acquainted with acceleration techniques [26]. The first step to accelerate intersection computations consists of enclosing each polygon into a rectangular bounding box. A further improvement consists of creating a hierarchical structure of bounding boxes that contain groups of bounding boxes. In this way, only the bounding boxes that are pierced by the rays are considered, therefore greatly reducing the number of intersection calculations. A final improvement consists of introducing the so called painter's algorithm that simply consists of keeping track of the objects that have a line of sight with the point of view and neglecting those that are shadowed by the closest ones.

3.3 The graph theoretical model

For the environment shown in Figure 8(a) one could draw a graph that collects all the visibility information obtained for each scattering element. The information is presented in Figure 8(b) and it represents a collection of elements that have a line of sight among each other. The process of the determination of the trajectories can be thought of as the extraction of the paths of Figure 8(b) that connect S with O . Because of the reasons

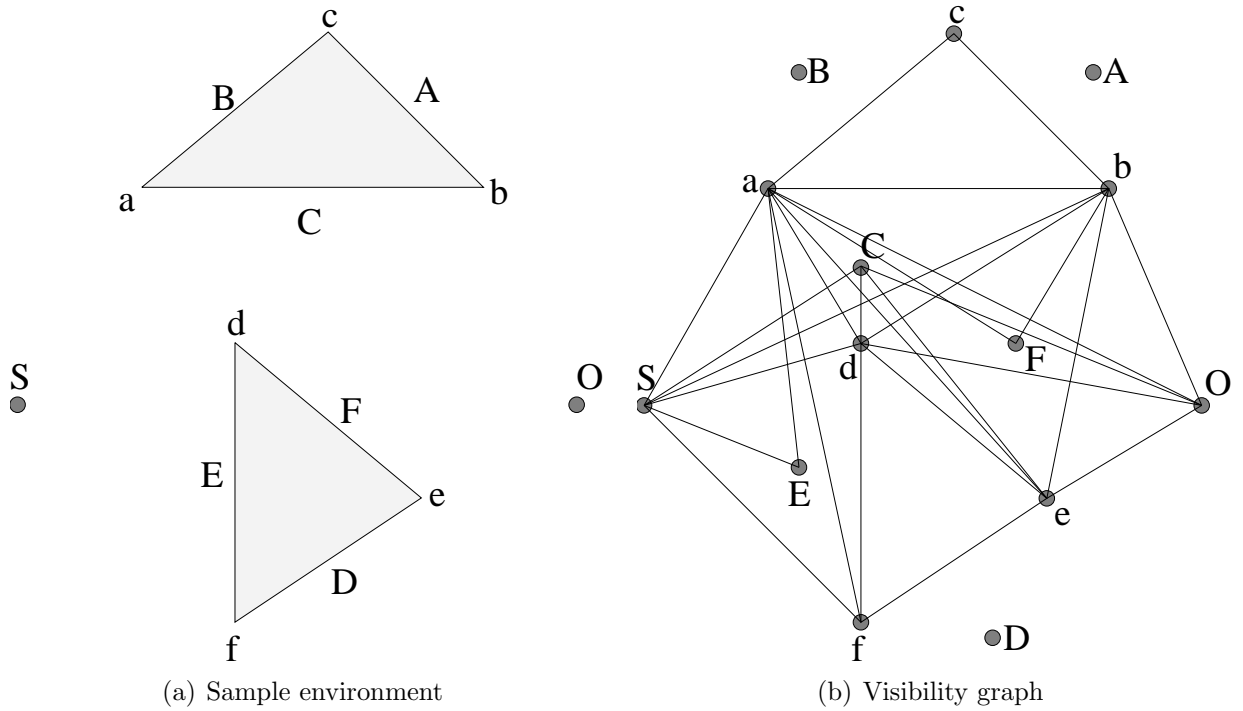
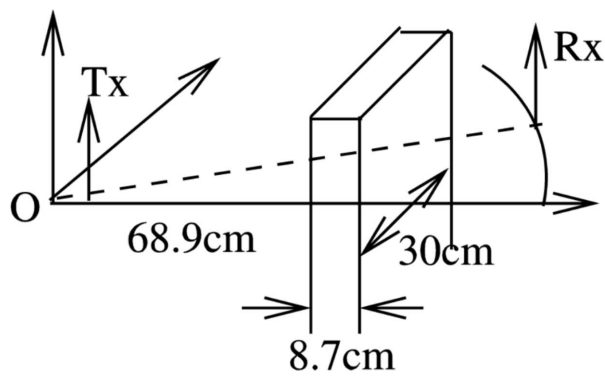


Figure 8: Sample 2D environment and corresponding visibility graph

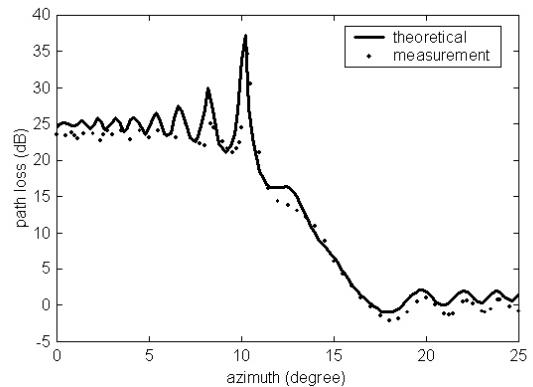
previously explained, all paths containing at least one reflection need to be checked to assess whether they satisfy the reflection law.

4 A new 3D propagation method

In 3D situations, ray tracing methods [27] [28] become very complicated because of the Keller's diffraction cone [8]. On the other hand, integral methods don't need tracing rays, but the computation increases tremendously when many buildings are present. However, using integral methods diffraction is usually considered only up to order 4, which makes it easier to implement them. Diffractions of higher orders usually become too weak to be important. Generally speaking, integral methods include solving parabolic equation (PE) with split-step Fourier transform [29], computing Fresnel-Kirchhoff integral by interpolation [30], [31], and applying asymptotic path-integral technique with repeated integral of the error function. The path-integral is equivalent to the Fresnel-Kirchhoff integral, but the repeated integral of error function is more time-consuming than the interpolation method. Here Fresnel-Kirchhoff integral is used to compute path loss from buildings in 3D urban and suburban environment (except downtown area), both diffraction and reflection are considered. An example of a perfectly conducting building as shown in Figure 9(a) is considered. The coordinates of the transmitter are (25.2cm, 0, 46cm). The building first intersects the x axis at $x=68.9\text{cm}$, and ends at $x=68.9\text{cm}+8.7\text{cm}$. The width and height of the building is 30cm and 50cm, respectively. The receiver moves along an arc centered at the origin with a radius of 114.8cm. The height of the receiver is 40cm. In the case of vertical polarization,



(a) Single building block



(b) Path loss

Figure 9: Path loss computation for a 3D environment obtained with the Fresnel method and comparison with measurements

the reflection coefficient of the roof and vertical walls is $+1$ and -1 . The reflection from the ground is neglected. At frequency of 50GHz , theoretical prediction of the path loss at the receiver (solid line) is compared with the measurement (dashed line) made in [32] as in Figure 9(b). The agreement between the prediction and the measurement is very good.

5 Conclusion

Our efforts in the development of the two-dimensional polygonal line simulator lead to very successful comparisons with measurements. Additionally, our efforts in developing 3D propagation simulators show promising results.

6 Acknowledgement

The authors would like to acknowledge Umberto G. Crovella, Giuseppe D'Elia, Dr. T. Monte, the UIC machine shop, the support of the Andrew Foundation, and the U.S. National Science Foundation that sponsored part of this research under grant ECS 9979413.

References

- [1] W. C. Jakes, *Microwave mobile communications*, IEEE Press, New York, 1974.
- [2] L. D. Parsons, *The mobile radio propagation channel*, Pentech Press, 1992.
- [3] T. S. Rappaport, *Wireless communications: principles and practice*, Prentice Hall, 1996.
- [4] H. L. Bertoni, *Radio propagation for modern wireless systems*, Prentice Hall, 2000.

- [5] M. F. Levy, *Parabolic equation methods for electromagnetic wave propagation*, Inspec/Institution of Electrical Engineers, 2000.
- [6] N. Blaunstein, *Radio propagation in cellular networks*, Artech House, 2000.
- [7] R. Janaswamy, *Radiowave propagation and smart antennas for wireless communications*, Kluwer Academic Publishers, 2001.
- [8] R. G. Kouyoumjian and P. H. Pathak, “A uniform geometrical theory of diffraction for an edge in a perfectly conducting surface,” *Proc. IEEE*, vol. 62, no. 11, pp. 1448–1461, Nov 1974.
- [9] D. Erricolo and P. L. E. Uslenghi, “Knife edge versus double wedge modeling of buildings for ray tracing propagation methods in urban areas,” in *Digest of National Radio Science Meeting*, Boulder, CO, USA, Jan 1998, p. 234.
- [10] D. Erricolo, “Experimental validation of second order diffraction coefficients for computation of path-loss past buildings,” *IEEE Transactions on Electromagnetic Compatibility*, vol. 44, no. 1, pp. 272–273, Feb. 2002.
- [11] M. Albani, F. Capolino, S. Maci, and R. Tiberio, “Diffraction at a thick screen including corrugations on the top face,” *IEEE Trans. Antennas Propagat.*, vol. 45, no. 2, pp. 277–283, Feb. 1997.
- [12] M. I. Herman and J. L. Volakis, “High frequency scattering by a double impedance wedge,” *IEEE Trans. Antennas Propagat.*, vol. 36, no. 5, pp. 664–678, May 1988.
- [13] D. Erricolo, G. D’Elia, and P.L.E. Uslenghi, “Measurements on scaled models of urban environments and comparisons with ray-tracing propagation simulation,” *IEEE Trans. Antennas Propagat.*, vol. 50, no. 5, pp. 727–735, May 2002.
- [14] D. Erricolo, U. G. Crovella, and P.L.E. Uslenghi, “Time-domain analysis of measurements on scaled urban models with comparisons to ray-tracing propagation simulation,” *IEEE Trans. Antennas Propagat.*, vol. 50, no. 5, pp. 736–741, May 2002.
- [15] J. Walfisch and H. L. Bertoni, “A theoretical model of UHF propagation in urban environments,” *IEEE Trans. Antennas Propagat.*, vol. 36, no. 12, pp. 1788–1796, Dec 1988.
- [16] S. R. Saunders and F. R. Bonar, “Explicit multiple building diffraction attenuation function for mobile radio wave propagation,” *Electron. Lett.*, vol. 27, no. 14, pp. 1276–1277, July 1991.
- [17] M. J. Neve and G.B. Rowe, “Assessment of GTD for mobile radio propagation prediction,” *Elec. Lett.*, vol. 29, no. 7, pp. 618–620, Apri 1993.
- [18] Wei Zhang, “A wide-band propagation model based on UTD for cellular mobile radio communications,” *IEEE Trans. Antennas Propagat.*, vol. 45, no. 11, pp. 1669–1678, Nov 1997.

- [19] J. H. Whittaker, "A generalized solution for diffraction over a uniform array of absorbing half screens," *IEEE Trans. Antennas Propagat.*, vol. 49, no. 6, pp. 934–938, June 2001.
- [20] D. Erricolo and P.L.E. Uslenghi, "Comparison between ray-tracing approach and empirical models for propagation in urban environments," *IEEE Trans. Antennas Propagat.*, vol. 50, no. 5, pp. 766–768, May 2002.
- [21] A. M. Watson D. Har and A. G. Chadney, "Comment on diffraction loss of rooftop-to-street in cost-231 walfisch-ikegami model," *IEEE Trans. Veh. Technol.*, vol. 48, no. 5, pp. 1451–1542, Sept. 1999.
- [22] M. Hata, "Empirical formula for propagation loss in land mobile radio services," *IEEE Trans. Veh. Technol.*, vol. VT-29, no. 3, pp. 317–325, Aug 1980.
- [23] Y. Okumura, E. Ohmori, T. Kawano, and K. Fukuda, "Field strength and its variability in VHF and UHF land-mobile radio service," *Rev. Electr. Commun. Lab. (Tokyo)*, vol. 16, no. 9 and 10, pp. 825–873, 1968.
- [24] D. Erricolo and P. L. E. Uslenghi, "Graph-theoretical approach to multiple scattering by polygonal cylinders," in *Intl. Conf. on Electromagnetics in Advanced Application*, Turin, Italy, Sept 1999, pp. 155–159.
- [25] T. Whitted, "An improved illumination model for shaded display," *Commun. ACM*, vol. 23, no. 6, pp. 343–349, June 1990.
- [26] J. Arvo and D. Kirk, "A survey of ray tracing acceleration techniques," in *An introduction to ray tracing*, A. S. Glassner, Ed. Academic Press, 1989.
- [27] F.A. Agelet, F. P. Fontan, and A. Formella, "Fast ray tracing for microcellular and indoor environments," *IEEE Trans. Magn.*, vol. 33, no. 2, pp. 1484–1487, 1997.
- [28] Z. Q. Yun, Z. J. Zhang, and M. F. Iskander, "A ray-tracing method based on the triangular grid approach and application to propagation prediction in urban environments," *IEEE Trans. Antennas Propagat.*, vol. 50, no. 5, pp. 750–758, May 2002.
- [29] L. Saini and U. Casiraghi, "A 3D fourier split-step technique for modeling microwave propagation in urban areas," in *Fourth European Conference on Radio Relay Systems*, 1993, pp. 210–214.
- [30] J. H. Whittaker, "Fresnel-kirchhoff theory applied to terrain diffraction problems," *Radio Sci.*, vol. 25, no. 5, pp. 837–851, Sept-Oct 1990.
- [31] T. A. Russell, C. W. Bostian, and T. S. Rappaport, "A deterministic approach to predicting microwave diffraction by buildings for microcellular systems," *IEEE Trans. Antennas Propagat.*, vol. 41, no. 12, pp. 1640–1649, Dec 1993.
- [32] G. A. J. van Dooren and M. H. A. J. Herben, "Polarisation-dependent site-shielding factor of block-shaped obstacle," *Electron. Lett.*, vol. 29, pp. 15–16, 1993.